REVIEWS

Journal of Semiconductors
(2023) 44, 091604
doi: 10.1088/1674-4926/44/9/091604

Organic-inorganic halide perovskites for memristors

Memoona Qammar, Bosen Zou, and Jonathan E. Halpert†

Department of Chemistry, Hong Kong University of Science and Technology (HKUST), Clear Water Bay Road, Kowloon 999077, Hong Kong SAR, China

Abstract: Organic-inorganic halides perovskites (OHPs) have drawn the attention of many researchers owing to their astonishing and unique optoelectronic properties. They have been extensively used for photovoltaic applications, achieving higher than 26% power conversion efficiency to date. These materials have potential to be deployed for many other applications beyond photovoltaics like photodetectors, sensors, light-emitting diodes (LEDs), and resistors. To address the looming challenge of Moore's law and the Von Neumann bottleneck, many new technologies regarding the computation of architectures and storage of information are being extensively researched. Since the discovery of the memristor as a fourth component of the circuit, many materials are explored for memristive applications. Lately, researchers have advanced the exploration of OHPs for memristive applications. These materials possess promising memristive properties and various kinds of halide perovskites have been used for different applications that are not only limited to data storage but expand towards artificial synapses, and neuromorphic computing. Herein we summarize the recent advancements of OHPs for memristive applications, their unique electronic properties, fabrication of materials, and current progress in this field with some future perspectives and outlooks.

Key words: organic-inorganic halide perovskites; resistive switching; memristors

Citation: M Qammar, B Zou, and J E. Halpert, Organic-inorganic halide perovskites for memristors[J]. *J. Semicond.*, 2023, 44(9), 091604. https://doi.org/10.1088/1674-4926/44/9/091604

1. Introduction

A memristor, a hybrid of memory and a resistor, can be understood as a two-terminal resistive switching (RS) device. The theoretical concept of memristors was introduced in 1971 by Leon Chua[1] as the fourth basic circuit component along with the known fundamental components of resistors, capacitors, and inductors, which give the relationship between magnetic flux (ϕ) and charge (q). All four elements of two terminal circuits and their relevant circuit variables are depicted in Fig. 1(a). Chua believed that logically there should be the missing circuit component with a magnitude that is a derivative of ϕ and q but the mystery of the memristor remained unresolved for the next 37 years. Finally, in 1962 Hickmott observed a sharp decrease in resistance across varying voltages when metal oxide films were sandwiched between metals[2]. This mechanism was dubbed resistive switching (RS) and devices exhibiting this phenomenon were called RS devices. In 2008 the first physical memristor was developed by Strukov *et al.* at Hewlett-Packard (HP) labs[3]. All non-volatile memory devices were declared to be memristors in 2011, and the current–voltage (I–V) graph was determined to be adequate to confirm a memristive phenomenon in any RS material[4]. A general metal–insulator–metal (MIM) structure of a typical memristor are shown in Fig. 1(b). Memory resistors are promising candidates to deal with the Von Neumann bottleneck by operating and storing the data on the same platform. They have proven to be useful in different fields like memory computing, neuromorphic computing, bioinspired computing, and information storage[5]. Essential characteristics of a memristor include high scalability, fast switching speed (~ps), high endurance, low operating voltage, and low power consumption (~fJ/bit)[6]. So far different materials comprised of chalcogenides[7–10], metal oxides[11–14], perovskites[15–17], and many others have been deployed for memristive applications.

Metal halide perovskites are one such promising class of materials, with several possible applications. Perovskites have a general formula ABX_3 (Fig. 1(c)) where A and B represent organic or inorganic cations and X is a halide, F, Cl, Br or I. They possess a 3D framework in which the A site cation is surrounded by a corner-sharing $[BX_6]$ octahedron[18]. For organic-inorganic halides perovskites (OHPs), the A site corresponds to an organic cation i.e., methylammonium (MA), formadinium (FA), ethyl ammonium (EA), etc. and the B site corresponds to inorganic bivalent cations like Pb^{2+} or Sn^{2+} and X^- is a halide ion. Currently, OHPs have achieved a breakthrough in photovoltaic applications by dint of their astonishing optoelectronic properties such as an adjustable bandgap, long (micrometer scale) carrier diffusion lengths, large absorption coefficients, and charge carrier mobilities[19]. In OHPs mixed ionic and electronic conduction is observable along with photosensitivity and their ionic conduction mechanism make them suitable for memristive applications[17, 20]. Since the observation of the memristive effect in $MAPbI_3$, many researchers are digging to unveil the properties and potential OHPs for further memristive applications[21].

Here we have reviewed the OHP-based memristors with a particular focus on the recent advancements in this area followed by the memristive mechanisms and some challenges. This review has the following structure. Section 2 will discuss the general memristive mechanism followed by the key find-

Correspondence to: J E. Halpert, jhalpert@ust.hk
Received 20 JUNE 2023; Revised 18 AUGUST 2023.

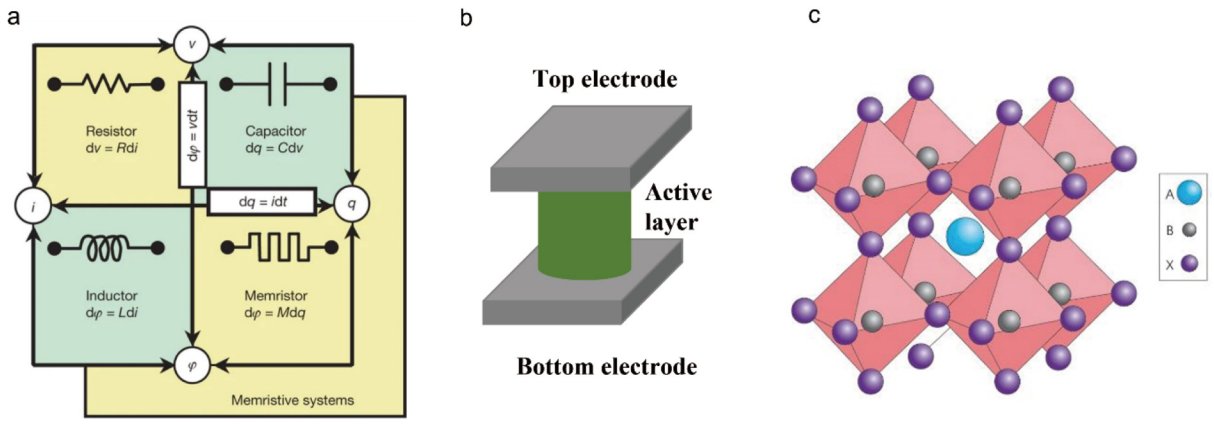

Fig. 1. (Color online) (a) The basic four elements of an electrical circuit. Reproduced with permission from Ref. [3]. Copyright 2008, Nature publisher. (b) MIM structure of a memristor. (c) ABX_3 structure of perovskite (A and B: cations and X: anion). Reproduced with permission from Ref. [18]. Copyright 2014, Nature publisher.

ings of different OHP-based memristors including 3D, 2D, and nanomaterials. Last section will cover the discussion about the challenges and future recommendations.

2. Key findings

2.1. Memristive mechanisms in OHPs

Since the discovery of first halide perovskite memristor, many types of OHPs have been explored for memristive applications and their performance parameters are summarized in Table 1. It is necessary to understand the mechanism underlying the RS in OHPs in order to achieve further progress in device design and performance. Commonly there are two types of RS observed in memristors: filamentary RS and interface type RS. There are many mechanisms proposed for memristors but for the memristors based on OHPs ion migration and charge trapping/de-trapping mechanisms are most widely reported[22]. In OHPs ionic migration can result from the migration of halide ions, interstitials, vacancies or metallic ions. An undesirable hysteresis is observed in OHP solar cells on account of defects/vacancies and ionic migration.

The ionic drifting (I^- and MA^+) in $MAPbI_3$ under influence of an external electric field is shown in the literature; for example Gu *et al.* proposed this method of RS in the first flexible $MAPbI_3$-based memristor[23] by fabricating a spin-cast $MAPbI_3$ thin film on a flexible plastic substrate. Space charge limited current (SCLC) and ohmic current were responsible for the switching and the conduction filament was generated due to an iodine donor vacancy defect (V_I), rather than lead and methylammonium acceptor vacancy defects (V_{Pb} and V_{MA}). The mechanism for the phenomena is presented in Figs. 2(a) and 2(b). The activation energy of formation of V_I is 0.58 eV and is the lowest among other defects and they can easily move along an octahedral edge in the perovskite structure. Later Zhu *et al.* used energy dispersive X-ray (EDX) to study the memristive mechanism in $MAPbI_3$[24]. They fabricated a planer memristor with Ag/$MAPbI_3$/Ag structure (Fig. 2(c)) and studied the elemental distributions at four different positions in Figs. 2(d) and 2(e). Prior to switching the I and Pb concentration was uniform but a reduction in I signals was observed when the device was under low resistance state (LRS), and this fact supports I^- migrationLRS), and this fact supports I^- migration[24]. Additional studies were carried out via X-ray photoelectron spectroscopy (XPS). In the LRS stage, AgI_x is formed and can be confirmed by observation of I^- 3d peaks. AgI_x can be generated by the reaction I^- with a metallic electrode thus generating (iodide vacancies) V_I which eventually form the conduction filament (CF) during SET operation. While resetting I^- can react with vacancies and break the CF. Similarly, Kim *et al.* also used EDS to study the distribution of I^- during setting and resetting of Si/$MAPbI_3$/Ag memristor. They found uniform distribution of iodine at 0 V but negative bias resulted in accumulation of more I^- near top electrode and positive bias reversed the distribution again[25].

Electrochemical active metals i.e., Ag, Ti, Zn, Al, and Cu are used as electrodes in OHPs and they can also participate in RS mechanism by making metallic CFs. This phenomenon was proposed by Yan *et al.*, where they observed memristive behavior by using active metals but only a typical resistor behavior with inert metals[26]. The role of the Ag filament for RS was supported by Yoo *et al.* and Wang *et al.*[27, 28]. Thickness-dependent memristive potential was studied for Ag/$MAPbI_3$/FTO[29]. According to this study, V_I CF and Ag CF compete but V_I CF are dominant in the thick-layered (300 nm) memristors. As the thickness is reduced to 90 nm, applied electric field would be enough to promote Ag CF formation[29]. The model for switching mechanism via Ag filament is shown in Figs. 2(f)–2(m). Apart from ion and defect migration, interfacial traps are also possible causes of RS. Zhou *et al.* studied $CH_3NH_3PbI_{3-x}Cl_x$ as an insulating material in memristors and proposed an interface-based RS mechanism[30]. The proposed mechanism is presented in Fig. 2(n). From ultraviolet photon spectroscopy (UPS) analysis, the work function of the active layer was 4.37 eV and the hole traps are located near the valence band. When the memristor is positively biased, hole injection takes place from the Au electrode to the trapping states which results in lowering the Schottky barrier and thus the memristor switches to a LRS. In case of negative bias, the Schottky barrier increases, removing holes and switching back to a HRS. Further studies show that energy consumption could be reduced by a photo assistance and the SET voltage was lowered to 0.1 V[30].

2.2. Memristive materials

2.2.1. 3-dimensional materials

Since 2015, 3D OHPs thin films have been most commonly used for memristor applications. Where Yoo *et al.*

Table 1. Summary of device performances of some OHP based memristors.

Structure	Method of synthesis	Structure	ON/OFF ratio	V_{on} (V)	V_{off} (V)	Endurance	Retention (s)	Mechanism	Ref
FTO/$MAPbI_{3-x}Cl_x$/Au	Solution method	3D	4	0.8	-0.6	$>10^3$	$>4\times10^4$	Ag conductive filament	[31]
PET/ITO/$MAPbI_3$/Au_3	Antisolvent assisted spin coatAntisolvent assisted spin coating 3D	50	0.7	-0.5	400	10^4	Defect migration	Defect migration	[23]
FTO/c-TiO_2/ $MAPbI_{3-x}Cl_x$/Al	Spin coating	3D	1.9×10^9	1.10	−1.65	–	–	Active metal filament	[26]
FTO/$CH_3NH_3PbI_3$/W	Antisolvent assisted spin coating	3D	>100	3.1	-1.1	>100	–	Schottky emission and ohmic conduction	[32]
ITO/PEDOT: PSS/$CH_3NH_3PbI_3$/ PCBM/Ag	Antisolvent assisted spin coating	3D	1.3×10^3	0.13	-0.23	10^3	–	Ion migration	[33]
PET/ITO/$MASnBr_3$/ Au	Antisolvent assisted spin coating	3D	100	0.65 ± 0.15 V	−3.1 ± 0.6 V	200	10^4	Formation and deformation of V_{Br}	[34]
ITO/PEDOT:PSS/ $MAPbI_3$/Au	2 step spin coating	3D	200	–	–	500	–	–	[35]
ITO/$MA_3Bi_2I_9$/Cu	Chemical vapor deposition (CVD)	3D	10^4	1	−6.9	1.73×10^3	$>3\times10^5$	Active metal filament	[36]
EGaIn/$MAPbI_3$/ PEDOT: PSS/ITO	Antisolvent assisted spin coating	3D	4.3×10^3	0.69	−0.41	10^4	10^5	V_I migration	[17]
Si/SiO_2/Ti/Pt/ $BA_2MA_{n-1}Pb_nI_{3n+1}$/Ag	Antisolvent assisted spin coating	2D	10^7	0.4–1.2	−1.2 to −0.4	250	1.08×10^4	Ag or V_I CF	[37]
Graphene/ $(PEA)_2PbBr_4$/Au	Exfoliation	2D	10	+7.6	−1.0	100	10^3	V_{Br} CF	[38]
ITO/BA_2PbBr_4/Au	Vapor deposition	2D	2.4×10^3	3	−3	6 0	10^3	V_{Br} CF	[39]
Si/SiO_2/Ti/Pt/ $(PEA)_2Cs_3Pb_4I_{13}$/Ag	Spin coating	2D	10^9	0.40	−0.10	230	2×10^3	Ag CF	[40]
F40/$MAPbBr_{1.97}Cl_{1.03}$/ Ag	Spin coating	Nanoparticles	500	0.55	−0.5	250	1×10^3	Surface defects/grain boundaries generated due to Cl substitution	[41]
PET/ITO/PMMA/41APbBr$_3$ PeQDs: PMMA/PMMA/Ag	Spin coating	Quantum dots	$>10^3$	1	−1	–	4×10^3	Trap controlled SCLC	[42]
42u/$CH_3NH_3PbI_3$/Pt	Vapour deposition	–	$>10^3$	1	−1	500	$>10^5$	–	[43]

reported the first bifunctional RS device with FTO/$MAPbI_{3-x}Cl_x$/Au for non-volatile memory (NVM) applications. The device performance was remarkable presenting endurance ~10^4 s and retention for 10^3 cycles but the ON/OFF current ratio was 4 only[31]. Gu *et al.* reported a $MAPbI_3$-based memristor by depositing an active layer on a flexible substrate by using one step antisolvent assisted spin coating technique for the first time[23]. The ON/OFF ratio of the device sustained for >100 bending cycles. In this work, the thickness was reduced and results were improved as compared to the previous report. The improvement in memristive properties by using active metals like Ag, Cu, Ti, Zn, and Al instead of inert metals was reported by Yan *et al.* in 2016[26]. Using Zn and Al as top electrodes resulted in instantaneous switching secondly integration of compact titania (c-TiO_2) resulted in higher ON/OFF ratio (1.9×10^9)[26]. The role of bromide substitution in typical $MAPbI_3$ structure by using density functional theory (DFT) calculation was reported in 2017[44]. Br-substitution red-shifted the band gap of the insulating layer. Here they compared the set electric field (E_{set} = V_{set}/thickness) instead of V_{set} because the Br substitution resulted in a variety of film thickness. They found the lowest E_{set} of 3.44×10^4 V/cm for pure $MAPbBr_3$[44]. In 2018 Cai *et al.* studied the effect of oleic acid (OA) passivation on the memristive properties on FTO/$CH_3NH_3PbI_3$/W device[32]. The OA passivation reduced the defect concentration in the semiconducting material and the switching mechanism shifted to Schottky and ohmic conduction. The addition of OA played a vital role in stability of material and reduction of the leakage current[32]. Until 2021 $MAPbI_3$ was still the most studied per-

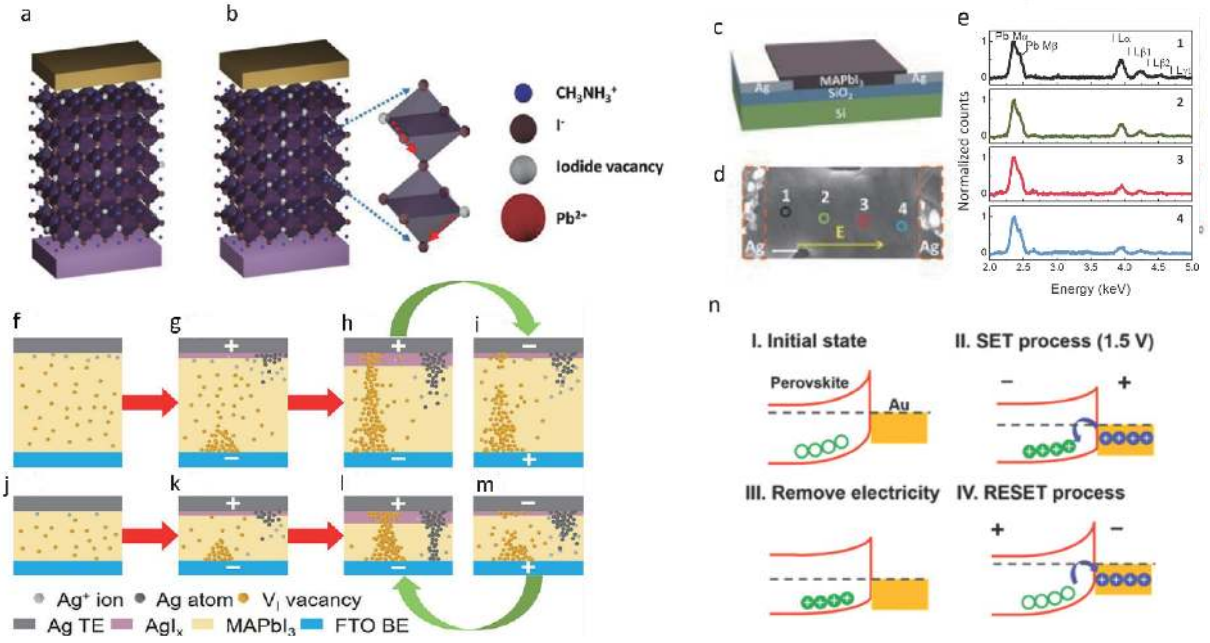

Fig. 2. (Color online) Different switching mechanisms in OHP memristors. (a) Iodide vacancies are arbitrarily distributed. (b) Iodide vacancies aligned under influence of applied voltage. Inset: Movement of vacancies along the octahedral edge of structure. Reproduced with permission from Ref. [23]. Copyright 2016, American Chemical Society. (c) Architecture of Ag/$MAPbI_3$/Ag device. (d) SEM micrograph showing 1–4 positions for EDS analysis. (e) EDS spectrum of device at LRS showing Pb and I peak intensities at four different positions shown in SEM image. Reproduced with permission from Ref. [24]. Copyright 2017, WILEY. Steps of RS via double-filament model in the Ag/$MAPbI_3$/FTO memory device. (f) The initial state (HRS), (g) forming, (h) SET (LRS), and (i) RESET process of the device with thick $MAPbI_3$ layer. (j) The initial state, (k) forming, (l) SET, and (m) RESET process of the device with relatively thinner $MAPbI_3$. Reproduced with permission from Ref. [29]. Copyright 2016, American Chemical Society. (n) Mechanism of electrical switching (Ⅰ) initial state corresponding to HRS: hole trapping centres locate at the perovskite surface; (Ⅱ) SET process: Hole trap states are filled, shifting the Fermi level to the valence band; (Ⅲ) remove light electricity: a lowered barrier and quasi ohmic contact are resulted corresponding to LRS; and (Ⅳ) electrical reset: Holes are extracted from the trap states and a transition from LRS to HRS occurs. Reproduced with permission from Ref. [30]. Copyright 2018, WILEY.

ovskite for RS applications, so Zhang *et al.* investigated into the effect of humidity on $MAPbI_3$-based memristor[45]. They fabricated an FTO/$MAPbI_3$/Au memristor by using a two-step spin coating method. Grain boundaries play an important role in facilitating ion migration while also, unfortunately, facilitating moisture ingression in the films. The LRS of the memristor decreases under moderate humidity (<75%) due to incorporation of H_2O molecules that are responsible for suppressing the iodide vacancies (V_I). This exploration exhibited that the $MAPbI_3$ layer could not tolerate humidity around 95% and quickly dissolved within 3 min[45]. That study proved the utilization of memristors for humidity and security sensitivity applications[45]. Gogoi *et al.* studied the effect of device scaling and characterization parameters like compliance current (I_{cc}), pulse width, frequency and voltage scan rate etc. for ITO/PEDOT: PSS/$MAPbI_3$/PCBM/Ag. As I_{cc} increased from 0.1 to 10 mA ON/OFF and V_{RESET} changed from 17 to 225 and 0.11 to 0.40 V respectively. The higher voltage scan rates resulted in higher values of V_{SET}/V_{RESET} and reset current values[33]. This study provided insight on the importance of measurement parameters for improvement of RS devices. For example, an increase in pulse parameters (amplitude and width) improved ON/OFF ratios and device scaling significantly affected the HRS values[33]. The device results observed under best parameters are summarized in Table 1. In 2019, for the first time a lead free $Cs_2AgBiBr_6$ double perovskite was unveiled for memristive applications[46]. Typically, they synthesized $Cs_2AgBiBr_6$ powder and solution casted it on top of ITO substrates assisted by low pressure to obtain pin hole free and uniform thin films[46]. These devices were environmentally robust by showing astonishing thermal and mechanical stability. They sustained their memristive abilities, retention ~10^5 even after 10 000 bending cycles, exposure to 80% humidity and high temperatures up to 453 K[46]. In 2020, OHPs based lead free flexible memristors with poly(ethylene terephthalate) PET/ITO/$MASnBr_3$/Au for multilevel information storage were reported by Qian *et al.*[34]. Other than typical ReRAM applications, $MAPbI_3$[35] and $MAPbBr_3$[47] based RS devices have also been explored for synaptic applications. Poddar *et al.* reported $MA_3Bi_2I_9$ for ReRAM by fabricating a uniform and pin hole free perovskite layer using a solvent free methodology[36]. This device outperformed all previously reported OHP thin films-based ReRAM devices by achieving the ultrafast switching speed of 10 ns for writing and erasing steps owing to rapidly developed conductive filament due to readily available Cu ions[36]. The variation in switching resistances before and after application of a 10 V/–10 V pulse for 10 ns for both the write and erase stages, respectively, as depicted in Figs. 3(a) and 3(b). Secondary ion mass spectroscopy (SIMS) was deployed to verify the conduction mechanism and the role of Cu in switching mechanism. The amount of Cu was higher in the bulk layer for the switched device as compared to unswitched device, thus supporting the mechanism of bridging Cu ions giving rise to the LRS[36].

Since $MAPbI_3$-based memristors suffer from environmental stability issues, researchers are striving to improve their sta-

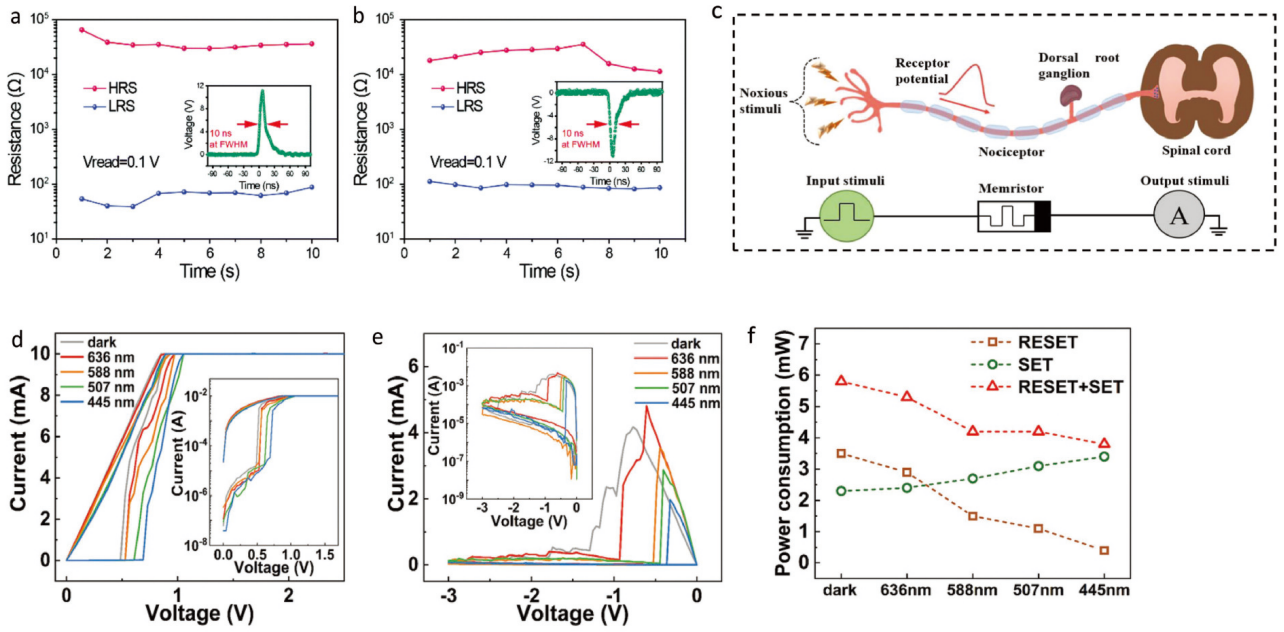

Fig. 3. (Color online) High and low resistance states of MBI ReRAM under influence of 10 ns, (a) 10 V writing pulse, (b) -10 V erasing pulse. Insets show the incident writing and erasing voltage pulse. Reproduced with permission from Ref. [36]. Copyright 2021, Royal Society of Chemistry. (c) Schematic illustration of biological (top) and artificial (bottom) nociceptor. Reproduced with permission from Ref. [49]. Copyright 2023, American Chemical Society. RS trend in EGaIn/$MAPbI_3$/PEDOT: PSS/ITO (d) SET process and (e) RESET process in dark and in presence of different wavelengths: 636, 588, 507, and 445 nm. Insets show the logarithmic scales of the same processes. (f) Power consumption for SET, RESET and total power consumption under the influence of different light signals. Reproduced with permission from Ref. [17]. Copyright 2023, WILEY.

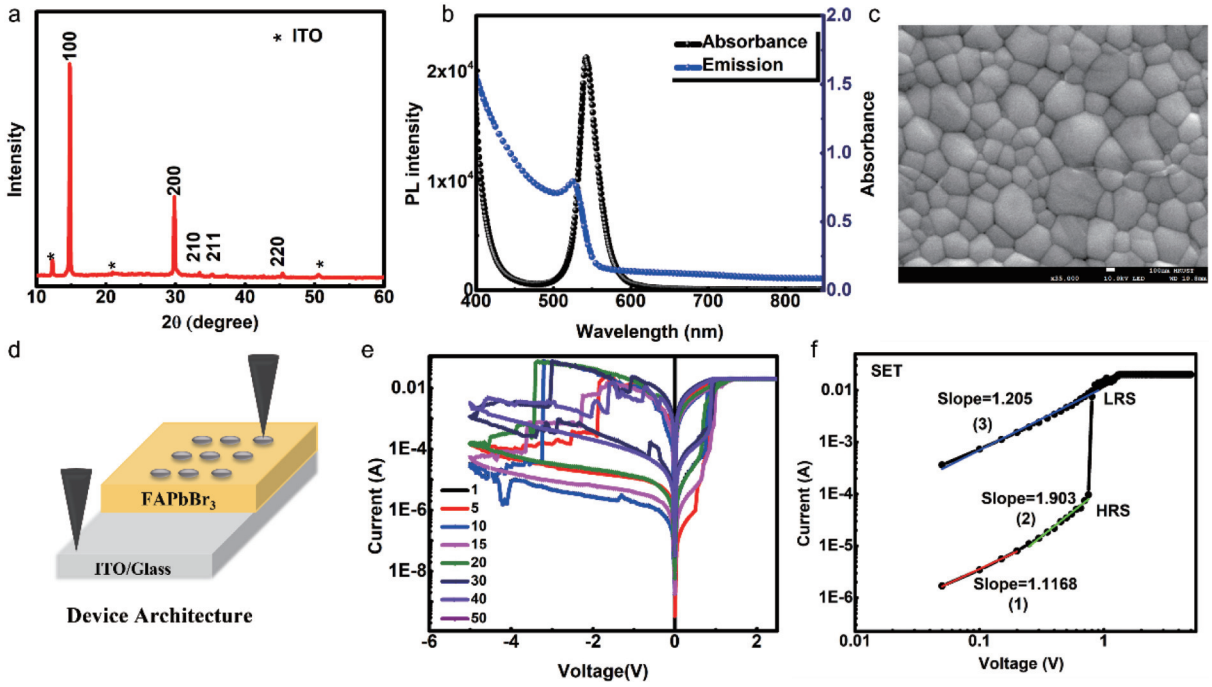

Fig. 4. (Color online) Material characterization of $FAPbBr_3$. (a) XRD, (b) UV-VIS and PL spectra, (c) SEM micrograph, (d) device design, (e) RS cycles for as fabricated device, and (f) conductive mechanism via measured and fitted curve for SET state.

bility against environmental effects. $FAPbBr_3$ is quite environmentally stable and has been previously used for various optoelectronic properties[48]. Here we have used a modified antisolvent assisted one-step spin coating method to obtain a dense, uniform, continuous and pin hole free thin film and then used in an MIM structure: ITO/$FAPbBr_3$/Ag. The successful synthesis of a semiconducting layer was tested by preliminary characterization techniques and results are depicted in Figs. 4(a)–4(d). The resistive switching of Ag/$FAPbBr_3$/ITO device (*I*–*V* curve) can be traced and reproduced 50 times, as demonstrated by the *I*–*V* curves shown in Fig. 4(e). There is only a very small deformation between subsequent switching cycles and set fail phenomena show that RS failure was not observed during the resistive switching of the dc voltage. The conduction mechanism for the SET state was analyzed from fitted results. The HRS consists of two regions, where

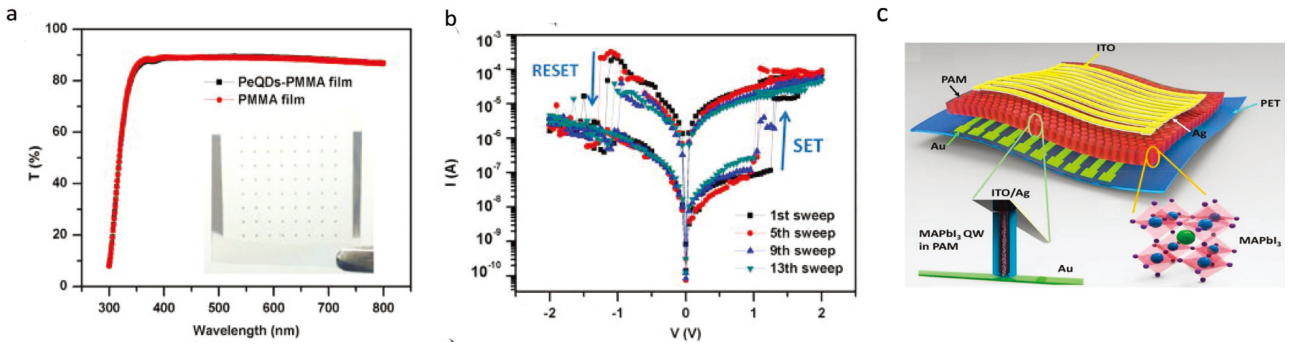

Fig. 5. (Color online) (a) Transmission spectra of pristine PMMA film and $MAPbBr_3$ QDs with a complete device shown in inset. (b) RS cycles of $MAPbBr_3$ QDs based memristor. Reproduced with permission from Ref. [42]. Copyright 2017, AIP Publishing. (c) Device architecture of $MAPbI_3$ QWs/NWs on PET substrate with an enlarged view of QW sandwiched between Ag and Au and crystal structure of $MAPbI_3$. Reproduced with permission from Ref. [50]. Copyright 2021, American Chemical Society.

region 1 corresponds to the Ohmic conduction ($I \propto V$) and region 2 corresponds to Child's law and supports the conduction via SCLC (space charge limited current) owing to charge trapping/detrapping. While LRS region is majorly dominated by Ohmic region and supports the CF formation between top and back electrodes (Fig. 4(f)).

Recently, in 2023 an OHP based diffusive memristor for artificial nociceptors has been presented for the first time. Patil *et al.* fabricated a memristor with Pd/$MAPbI_3$/ITO device architecture by using a typical one step antisolvent-assisted spin coating technique[49]. The device exhibited ON/OFF around 10^4 and endured $>10^2$ bending cycles. The device emulated the figure of merits of pain receptors like threshold, relaxation, and no adaptation against the pulse provided. Schematic illustration of biological and artificial nociceptors is shown in Fig. 3(c)[49]. An improvement in switching properties of $MAPbI_3$ due to photo-influence is investigated by Liu *et al.* very recently[17]. Where they fabricated a sandwiched (eutectic gallium and indium) EGaIn/$MAPbI_3$/PEDOT: PSS/ITO device architecture. The key parameters of the device under consideration were significantly improved by using light (445 nm) illumination so that a 34% drop in power consumption was observed along with a long data retention time of 10^5 s. The photo induced effect on the resistive switching and power consumption are presented in Figs. 3(d)–3(f). The memristive mechanistic studies were carried out and the switching behavior was attributed to V_I conduction filaments that were evidenced from cross-sectional SEM studies.

2.2.2. 2D materials

Despite the rapid progress in the field of memristive applications deploying 3D OHP perovskites, this field is still facing a challenging situation to tackle with the phase and environmental instability of 3D perovskites[51]. To mitigate these issue researchers suggested that inorganic counterparts like Cs or Rb can be deployed[52, 53]. Apart from moving to all inorganic perovskites, utilization of low dimensional materials can also be a potential solution to conquer these problems[54]. Perovskites with lower dimensionality possess higher stability, lesser grain boundaries and lower trap densities as compared to their 3D counterparts so many low dimensional OHP have been tried for memristive applications[55–57]. The first report on 2D memristor with $Si/SiO_2/Ti/Pt/$ (BA: Butylammonium) $BA_2MA_{n-1}Pb_nI_{3n+1}$/Ag device structure was dated back in 2017[37]. Seo *et al.* compared the performance of 2D OHP with quasi-2D and 3D perovskite. The V_{SET} for 2D was quite lower than other counterparts and ON/OFF was improved from 10^2 to 10^7 owing to increased Schottky barrier heights[37]. After that, Tian *et al.* recorded a millimeter sized 2D memristor (Graphene/$(PEA)_2PbBr_4$/Au). The device exhibited ultra-low operating current of 0.1 pA only thus proving its potential for ultra-low energy consumption devices[38]. Later, Cheng *et al.* observed ternary switching in 2D $(CH_3NH_3)2PbI_2(SCN)_2$ based memristors. The devices exhibited terrific endurance, flexibility and retention[58]. Later, Lee *et al.* studied how grain size influences the memristive properties of BA_2PbBr_4. They fabricated thin films by using vapor deposition technique and varied the grain sizes by manipulating the deposition temperature. As the grain size improved ON/OFF improved to 2.4×10^3 [39]. In the following year, Kim *et al.* explored memristive characteristics of a quasi-2D material in $Si/SiO_2/Ti/Pt/(PEA)_2Cs_3Pb_4I_{13}$/Ag device. As compared to bulk 3D $CsPbI_3$, it was moisture resistant and retained a high ON/OFF ratio for 2 weeks under ambient conditions[40].

2.2.3. Nanostructures for memristors

Muthu *et al.* explored mixed anion OHP nanoparticles as memristors by spin-coating Cl doped nanoparticles on FTO coated glass substrate[41]. The role of anionic substitution was found crucial because additional chloride anion increased the defects in the system and thus resulted in improvement of ON/OFF to 5×10^2 [41]. However, a pure $MAPbBr_3$ perovskite QD (PeQD) memristor fabricated by using the spin coating method was reported by Yang *et al.* in 2017[42]. This device used PeQDs with a size distribution of 5–10 nm and structure of PET/ITO/PMMA/$MAPbBr_3$ PeQDs: PMMA/PMMA/Ag. The good transparency of the film was seen via visible light and ON/OFF ratio of 10^3 was observed. The transmission spectra and *I*–*V* graph of the film are given in Figs. 5(a) and 5(b)[42]. In the same year, another study was reported to deposit OHP memristors onto the nanoholes using vapor deposition method that is not possible to carry out using conventional procedures[43]. They achieved a uniform layer of $MAPbI_3$ on the nano template. The reproductive RS behavior between HRS and LRS was recorded by the device[43]. Zhao *et al.* reported 1D memristor based on $MAPbI_3$ nanofibers however the device showed inferior RS value and showed degradation during aging process due to redox reaction[59]. 0D $MAPbBr_3$ NCs were synthesized by Jie *et al.* by the typical solution method. This device showed a high ON/OFF ratio of 10^8,

good stability, a large hysteresis window of 77.4 V and increased conductance with increase in gate voltage[60]. Later, $MAPbI_3$ based memristor having structure of Au (40 nm)/$MAPbI_3$ (440 nm)/indium tin oxide (ITO, 300 nm) was prepared using solution process. They fabricated an artificial neuron and the change in its electrical properties mimicked a real neuron. This memristor was able to modulate its properties smoothly and continuously and took over 1000 states. Also, an excellent amplitude-frequency response was observed[61]. In 2021 Poddar *et al.* studied the quantum wires (QWs) and nanowires (NWs) made of $MAPbI_3$ perovskite as solid electrolyte and silver (Ag) as active electrode with the device structure given in Fig. 5(c)[50]. They reported that QWs and NWs showed electrical switching behavior due to Ag cation reduction at the aluminium counter-electrode. The resulting device showed 100 ps programming speed, endurance performance of up to 6×10^6 cycles without any significant degradation in ON/OFF ratio, and scalability down to ~14 nm lateral dimension[50]. Recently, Zhang *et al.* reported a study on $MAPbCl_3$ nanowires (NWs) to be used in ReRAMs[62]. They prepared Ag/$MAPbCl_3$ NWs/Al ReRAM and claimed the longest data retention performance among all the previously reported OHP-ReRAM systems[62]. There are not many reports on the nanoscale production of OHPs for ReRAM, and researchers are still struggling to achieve facile synthesis of these materials. Further studies are required to explore the nano-dimensional effect on the properties and device efficiency of the OHP materials.

3. Summary and perspective

OHP has been widely deployed for photovoltaic applications but some of their unique properties make the potential for optoelectronic applications beyond photovoltaics. OHPs can be declared as revolutionary materials for their utility as memristors and future electronics. In this work we have provided an overview of the progress of OHP-based memristors used in different applications, their working mechanisms and the type of OHPs used so far. They have achieved ON/OFF in order of 10^9 and low SET/RESET voltages[26, 40]. Apart from their versatile applications like ReRAM, logic gates, artificial synapses etc. they have some inevitable drawbacks including instability towards environmental effects and a limited understanding of the mechanism of memristive behavior. Most of the progress has been made with Pb-based OHPs but the toxicity of lead is an issue that cannot be avoided indefinitely. In conclusion, device performances using these material systems are improving rapidly, largely by refinements to the encapsulation, detailed mechanistic studies, and the use of lead-free "perovskite-like" materials. With further advances, these perovskite memristors may yet reach their ultimate potential and overcome Von Neumann's bottleneck.

References

[1] Chua L. Memristor-The missing circuit element. IEEE Trans Circuit Theory, 1971, 18, 507

[2] Hickmott T W. Low-frequency negative resistance in thin anodic oxide films. J Appl Phys, 1962, 33, 2669

[3] Strukov D B, Snider G S, Stewart D R, et al. The missing memristor found. Nature, 2008, 453, 80

[4] Chua L. Resistance switching memories are memristors. Handbook of memristor networks, 2019, 197

[5] Kim S, Du C, Sheridan P, et al. Experimental demonstration of a second-order memristor and its ability to biorealistically implement synaptic plasticity. Nano Lett, 2015, 15, 2203

[6] Chen W B, Song L K, Wang S B, et al. Essential characteristics of memristors for neuromorphic computing. Adv Elect Materials, 2023, 9, 2200833

[7] Cryer M E, Fiedler H, Halpert J E. Photo-electrosensitive memristor using oxygen doping in HgTe nanocrystal films. ACS Appl Mater Interfaces, 2018, 10, 18927

[8] Hu Z J, Cao F, Yan T T, et al. *In situ* vulcanization synthesis of $CuInS_2$ nanosheet arrays for a memristor with a high on–off ratio and low power consumption. J Mater Chem C, 2023, 11, 244

[9] Aabel P, Sai Guru Srinivasan S, Amiruddin R, et al. Bi-polar switching properties of FTO/CZTS/Ag device. J Mater Sci Mater Electron, 2023, 34, 1

[10] Li Y, Zhong Y P, Xu L, et al. Ultrafast synaptic events in a chalcogenide memristor. Sci Rep, 2013, 3, 1619

[11] Hu H R, Scholz A, Liu Y, et al. A fully inkjet-printed unipolar metal oxide memristor for nonvolatile memory in printed electronics. IEEE Trans Electron Devices, 2023, 70, 3051

[12] Sato K, Hayashi Y, Masaoka N, et al. High-temperature operation of gallium oxide memristors up to 600 K. Sci Rep, 2023, 13, 1

[13] Basnet P, Anderson E C, Athena F F, et al. Asymmetric resistive switching of bilayer HfO_x/AlO_y and AlO_y/HfO_x memristors: The oxide layer characteristics and performance optimization for digital set and analog reset switching. ACS Appl Electron Mater, 2023, 5, 1859

[14] Prezioso M, Merrikh-Bayat F, Hoskins B D, et al. Training and operation of an integrated neuromorphic network based on metal-oxide memristors. Nature, 2015, 521, 61

[15] Wu Y H, Huang H Y, Xu C, et al. The $FAPbI_3$ perovskite memristor with a PMMA passivation layer as an artificial synapse. Appl Phys A, 2023, 129, 1

[16] Guo Z C, Xiong R, Zhu Y Y, et al. High-performance and humidity robust multilevel lead-free all-inorganic $Cs_3Cu_2Br_5$ perovskite-based memristors. Appl Phys Lett, 2023, 122, 053502.

[17] Liu Z H, Cheng P P, Kang R Y, et al. Photo-enhanced resistive switching effect in high-performance $MAPbI_3$ memristors. Adv Materials Inter, 2023, 10, 2201513

[18] Green M A, Ho-Baillie A, Snaith H J. The emergence of perovskite solar cells. Nat Photonics, 2014, 8, 506

[19] Bati A S R, Zhong Y L, Burn P L, et al. Next-generation applications for integrated perovskite solar cells. Commun Mater, 2023, 4, 1

[20] DeQuilettes D W, Zhang W, Burlakov V M, et al. Photo-induced halide redistribution in organic–inorganic perovskite films. Nat Commun, 2016, 7, 1

[21] Xiao Z G, Yuan Y B, Shao Y C, et al. Giant switchable photovoltaic effect in organometal trihalide perovskite devices. Nat Mater, 2015, 14, 193

[22] Zhang C, Li Y, Ma C L, et al. Recent progress of organic–inorganic hybrid perovskites in RRAM, artificial synapse, and logic operation. Small Sci, 2022, 2, 2100086

[23] Gu C, Lee J S. Flexible hybrid organic–inorganic perovskite memory. ACS Nano, 2016, 10, 5413

[24] Zhu X J, Lee J H, Lu W D. Perovskite films: Iodine vacancy redistribution in organic-inorganic halide perovskite films and resistive switching effects. Adv Mater, 2017, 29, 1700527

[25] Kim D J, Tak Y J, Kim W G, et al. Resistive switching properties through iodine migrations of a hybrid perovskite insulating layer. Adv Mater Interfaces, 2017, 4, 1601035

[26] Yan K, Peng M, Yu X, et al. High-performance perovskite memristor based on methyl ammonium lead halides. J Mater Chem C, 2016, 4, 1375

[27] Yoo E, Lyu M Q, Yun J H, et al. Bifunctional resistive switching behavior in an organolead halide perovskite based Ag/

$CH_3NH_3PbI_{3-x}Cl_x$/FTO structure. J Mater Chem C, 2016, 4, 7824
[28] Wang W, Xu J Q, Ma H L, et al. Insertion of nanoscale AgInSbTe layer between the Ag electrode and the $CH_3NH_3PbI_3$ electrolyte layer enabling enhanced multilevel memory. ACS Appl Nano Mater, 2019, 2, 307
[29] Sun Y M, Tai M Q, Song C, et al. Competition between metallic and vacancy defect conductive filaments in a $CH_3NH_3PbI_3$-based memory device. J Phys Chem C, 2018, 122, 6431
[30] Zhou F C, Liu Y H, Shen X P, et al. Low-voltage, optoelectronic $CH_3NH_3PbI_{3-x}Cl_x$ memory with integrated sensing and logic operations. Adv Funct Mater, 2018, 28, 1800080
[31] Yoo E J, Lyu M Q, Yun J H, et al. Resistive switching behavior in organic-inorganic hybrid $CH_3NH_3PbI_{3-x}Cl_x$ Perovskite for resistive random access memory devices. Adv Mater, 2015, 27, 6170
[32] Cai H M, Ma G K, He Y L, et al. A remarkable performance of $CH_3NH_3PbI_3$ perovskite memory based on passivated method. Org Electron, 2018, 58, 301
[33] Gogoi H J, Mallajosyula A T. Enhancing the switching performance of $CH_3NH_3PbI_3$ memristors by the control of size and characterization parameters. Adv Elect Materials, 2021, 7, 2100472
[34] Qian W H, Cheng X F, Zhou J, et al. Lead-free perovskite $MASnBr_3$-based memristor for quaternary information storage. InfoMat, 2020, 2, 743
[35] Xiao Z G, Huang J S. Energy-efficient hybrid perovskite memristors and synaptic devices. Adv Electron Mater, 2016, 2, 1600100
[36] Poddar S, Zhang Y T, Zhu Y Y, et al. Optically tunable ultra-fast resistive switching in lead-free methyl-ammonium bismuth iodide perovskite films. Nanoscale, 2021, 13, 6184
[37] Seo J Y, Choi J, Kim H S, et al. Wafer-scale reliable switching memory based on 2-dimensional layered organic–inorganic halide perovskite. Nanoscale, 2017, 9, 15278
[38] Tian H, Zhao L F, Wang X F, et al. Extremely low operating current resistive memory based on exfoliated 2D perovskite single crystals for neuromorphic computing. ACS Nano, 2017, 11, 12247
[39] Lee D, Hwang B, Lee J S. Impact of grain sizes on programmable memory characteristics in two-dimensional organic–inorganic hybrid perovskite memory. ACS Appl Mater Interfaces, 2019, 11, 20225
[40] Kim H, Choi M J, Suh J M, et al. Quasi-2D halide perovskites for resistive switching devices with ON/OFF ratios above 10^9. NPG Asia Mater, 2020, 12, 21
[41] Muthu C, Agarwal S, Vijayan A, et al. Hybrid perovskite nanoparticles for high-performance resistive random access memory devices: Control of operational parameters through chloride doping. Adv Mater Interfaces, 2016, 3, 1600092
[42] Yang K Y, Li F S, Veeramalai C P, et al. A facile synthesis of $CH_3NH_3PbBr_3$ perovskite quantum dots and their application in flexible nonvolatile memory. Appl Phys Lett, 2017, 110, 083102
[43] Hwang B, Lee J S. A strategy to design high-density nanoscale devices utilizing vapor deposition of metal halide perovskite materials. Adv Mater, 2017, 29, 1701048
[44] Hwang B, Gu C, Lee D, et al. Effect of halide-mixing on the switching behaviors of organic-inorganic hybrid perovskite memory. Sci Rep, 2017, 7, 43794
[45] Zhang X H, Zhao X N, Shan X Y, et al. Humidity effect on resistive switching characteristics of the $CH_3NH_3PbI_3$ memristor. ACS Appl Mater Interfaces, 2021, 13, 28555
[46] Cheng X F, Qian W H, Wang J, et al. Environmentally robust memristor enabled by lead-free double perovskite for high-performance information storage. Small, 2019, 15, 1905731
[47] John R A, Yantara N, Ng Y F, et al. Ionotronic halide perovskite drift-diffusive synapses for low-power neuromorphic computation. Adv Mater, 2018, 30, 1805454
[48] Shivarudraiah S B, Tewari N, Ng M, et al. Optically clear films of formamidinium lead bromide perovskite for wide-band-gap, solution-processed, semitransparent solar cells. ACS Appl Mater Interfaces, 2021, 13, 37223
[49] Patil H, Kim H, Kadam K D, et al. Flexible organic–inorganic halide perovskite-based diffusive memristor for artificial nociceptors. ACS Appl Mater Interfaces, 2023, 15, 13238
[50] Poddar S, Zhang Y T, Gu L L, et al. Down-scalable and ultra-fast memristors with ultra-high density three-dimensional arrays of perovskite quantum wires. Nano Lett, 2021, 21, 5036
[51] Guan X W, Wan T, Hu L, et al. A solution-processed all-perovskite memory with dual-band light response and tri-mode operation. Adv Funct Materials, 2022, 32, 2110975
[52] Kulbak M, Gupta S, Kedem N, et al. Cesium enhances long-term stability of lead bromide perovskite-based solar cells. J Phys Chem Lett, 2016, 7, 167
[53] Le Q V, Lee J W, Sohn W, et al. Low temperature solution-processable cesium lead bromide microcrystals for light conversion. Cryst Growth Des, 2018, 18, 3161
[54] Guan X W, Lei Z H, Yu X C, et al. Low-dimensional metal-halide perovskites as high-performance materials for memory applications. Small, 2022, 18, 2203311
[55] Hu L, Zhao Q, Huang S J, et al. Flexible and efficient perovskite quantum dot solar cells via hybrid interfacial architecture. Nat Commun, 2021, 12, 466
[56] Yin J, Maity P, Naphade R, et al. Tuning hot carrier cooling dynamics by dielectric confinement in two-dimensional hybrid perovskite crystals. ACS Nano, 2019, 13, 12621
[57] Kim J, Hu L, Chen H J, et al. P-type charge transport and selective gas sensing of all-inorganic perovskite nanocrystals. ACS Mater Lett, 2020, 2, 1368
[58] Cheng X F, Hou X, Zhou J, et al. Pseudohalide-induced 2D $(CH_3NH_3)_2PbI_2(SCN)_2$ perovskite for ternary resistive memory with high performance. Small, 2018, 14, 1703667
[59] Zhao J, Li S J, Tong W C, et al. Light-induced anomalous resistive switches based on individual organic-inorganic halide perovskite micro-/ nanofibers. Adv Electron Mater, 2018, 4, 1800206
[60] Jiang T H, Shao Z B, Fang H, et al. High-performance nanofloating gate memory based on lead halide perovskite nanocrystals. ACS Appl Mater Interfaces, 2019, 11, 24367
[61] Yang J Q, Wang R P, Wang Z P, et al. Leaky integrate-and-fire neurons based on perovskite memristor for spiking neural networks. Nano Energy, 2020, 74, 104828
[62] Zhang Y T, Poddar S, Huang H, et al. Three-dimensional perovskite nanowire array–based ultrafast resistive RAM with ultralong data retention. Sci Adv, 2021, 7, eabg3788

Memoona Qammar got her bachelor's degree in chemistry from University of Sargodha Pakistan in 2014 and master's degree from National University of Sciences and Technology (NUST) Pakistan in 2017. Now she is a doctoral student at The Hong Kong University of Science and Technology (HKUST) Hong Kong under supervision of Prof. Jonathan Halpert. Currently, her work focusses on the optoelectronic properties of perovskites.

Jonathan E. Halpert received his PhD from the Massachusetts Institute of Technology (MIT) in 2008. He is currently an assistant professor in the Department of Chemistry at The Hong Kong University of Science & Technology (HKUST). His work is currently focused on optoelectronic devices made from perovskite and copper halide nanocrystals.